Mechanism of Oxidative Shuttling for [2]Rotaxane in a Stoddart−Heath Molecular Switch: Density Functional Theory Study with Continuum-Solvation Model

Yun Hee Jang[†] and William A. Goddard, III*

Materials and Process Simulation Center, Beckman Institute (139-74), California Institute of Technology, Pasadena, California 91125

Received: September 26, 2005; In Final Form: February 6, 2006

The central component of the programmable molecular switch demonstrated recently by Stoddart and Heath is [2]rotaxane, which consists of a cyclobis-(paraquat-*p*-phenylene) ring-shaped shuttle [$(CBPQT^{4+})(PF_6^-)_4$] encircling a finger and moving between two stations on the finger: tetrathiafulvalene (TTF) and 1,5-dioxynaphthalene (DNP). We report here a quantum mechanics (QM) study of the mechanism by which movement of the ring (and in turn the on−off switching) is controlled by the oxidation−reduction process. We use B3LYP density functional theory to describe how oxidation of the [2]rotaxane components (in using Poisson−Boltzmann continuum-solvation theory for acetonitrile solution) induces the motions associated with switching (translation of the ring). These calculations support the proposal that oxidation occurs on TTF, leading to repulsion between two positive charge centers (TTF^{2+} and $CBPQT^{4+}$) that drives the $CBPQT^{4+}$ ring from the TTF^{2+} station toward the neutral DNP station. The theory also supports the experimental observation that the first and second oxidation potentials are nearly the same (separated by 0.09 eV in the QM). This excellent agreement between the QM and experiment suggests that QM can be useful in designing new systems.

1. Introduction

One of the most promising candidates for a programmable molecular switch in molecular electronic devices[1−7] is a self-assembled monolayer (SAM) of the Stoddart−Heath type bistable [2]rotaxane (**1**) anchored between two electrodes.[2,4] (Alternatively, one might consider the [2]catenane relative.[8,9]) It is thought that this type of switch is turned on and off reversibly upon moving the cyclobis-(paraquat-*p*-phenylene) ($CBPQT^{4+}$; blue ring) shuttle between the tetrathiafulvalene (TTF; green station) and the 1,5-dioxynaphthalene (DNP; red station) by oxidation and reduction of the TTF.[10−12] However, the fundamental understanding of the switching behavior of **1** needed for deriving a design principle to improve switching components is still lacking,[1] especially for the solid-state devices.[4,13,14]

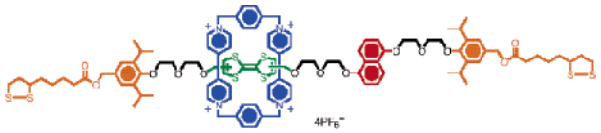

1

There have been theoretical studies on various models of **1**, using both quantum-mechanics (QM)[15−22] and force-field (FF)[23−29] approaches, but there has been little work to establish the origin of the on−off switching of [2]rotaxane.[15,17,18,23] Recently, we reported the electronic structures of the simplest models representing the basic components of **1** to establish the role of each component in conduction as a step toward understanding the switching behavior accomplished by changing the ring position.[18] The model components studied were all neutral; however, the shuttling and, in turn, the switching of **1** is controlled by the oxidation and reduction. Thus, we now report the behaviors (energetic and electronic changes) of the same components under the redox process, as the next step toward understanding the switching mechanism of **1**.

A specific question here is which part of **1** is really oxidized. The HOMO energy level of TTF is higher than that of DNP, so it is widely accepted that the oxidation of **1** occurs first on TTF, leading to TTF^+ upon the first oxidation and then to TTF^{2+} at the second oxidation. Consequently, one expects that the repulsion between two positive charge centers, TTF^{2+} and $CBPQT^{4+}$, would drive the $CBPQT^{4+}$ ring from the TTF^{2+} station to the *still neutral* DNP station, turning the switch on. This assumption was made in our previous calculations.[15,17,18]

On the other hand, our previous electronic structure calculations indicated that the CBPQT shuttle encircling TTF at the neutral state exerts a net electropositive field around TTF, pulling down its HOMO level significantly.[18] This is also implied by the electrochemical observation of a large shift of the first oxidation peak toward a more positive potential.[13,30,31] This should reduce significantly the gap between the two energy levels of **1**, the TTF-centered HOMO, and the DNP-centered HOMO−1. Moreover, a positive charge built up (presumably on TTF) after the first oxidation may also induce similar level shifts (shifting the TTF-centered HOMO level even lower).

This raises a question: Which configuration of **1** would be preferred upon the second oxidation, a [TTF^{2+}−DNP^0] type or a [$TTF^{\bullet+}$−$DNP^{\bullet+}$] type? Is it the TTF site that is doubly oxidized in **1** (the former), as widely accepted? Or is it two single oxidations, one on each of the two sites (the latter) that occurs? This latter description appears to be a good alternative for **1** to avoid the large amount of repulsion between TTF^{2+} and $CBPQT^{4+}$ in the first place.

* To whom correspondence should be sent (Phone 626-395-2731, Fax 626-585-0918, E-mail wag@wag.caltech.edu).

[†] Present addresses: Department of Materials Science and Engineering, Gwangju Institute of Science and Technology, Gwangju 500-712, Korea; LEMA, Université François Rabelais, 37200 Tours, France.

10.1021/jp055473c CCC: $30.25
Published on Web 03/28/2006

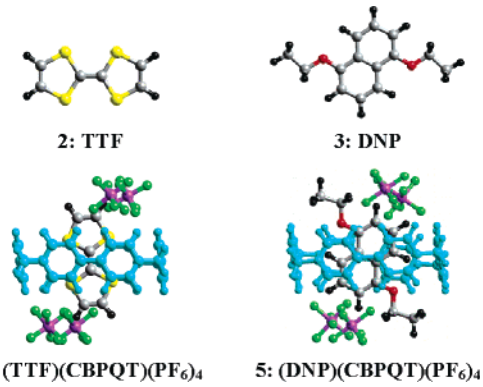

Figure 1. Key components of **1** calculated in our bottom-up model. Color code: yellow (S), red (O), gray (C), black (H), purple (P), light green (F), and light blue (CBPQT).

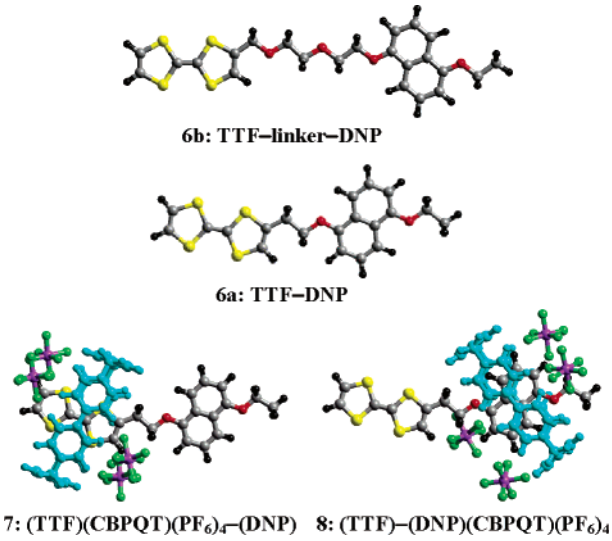

Figure 2. Simplest two-station models of **1**. Color code: yellow (S), red (O), gray (C), black (H), purple (P), light green (F), and light blue (CBPQT).

In this study, we revisit this basic question of *oxidation* and *shuttling* and confirm the prevailing assumption (the former case above). We use density functional theory (DFT; B3LYP) in combination with the Poisson−Boltzmann continuum-solvation model to study the neutral, oxidized (+1), and doubly oxidized (+2) states of key components in acetonitrile (AN) solution. We also calculate the reduction potentials to compare with cyclic voltametry (CV) experiments.

2. Method

2.1. Bottom-Up Model. Our previous work[18] has shown that the electronic structure of a two-station model of **1** can be described reasonably well by a simple sum of two stations calculated separately. We applied this *bottom-up* or *aufbau* approach again to examine the oxidation process of **1**.

The key components actually calculated are the following (Figure 1):

(a) each station, TTF (**2**) and DNP (**3**);
(b) the complex between the shuttle and each station, $(TTF)(CBPQT)(PF_6)_4$ (**4**) and $(DNP)(CBPQT)(PF_6)_4$ (**5**).

Then, the two-station species (dumbbell and [2]rotaxane; Figure 2) are treated as a sum of two stations:

(a) [**2** + **3**] for dumbbell **6**;
(b) [**4** + **3**] for [2]rotaxane *green* isomer **7** (ring on TTF);
(c) [**2** + **5**] for [2]rotaxane *red* isomer **8** (ring on DNP).

Thus, the key states of **1** are represented as follows:

(a) neutral dumbbell **6** by [**2** + **3**];
(b) oxidized dumbbell $\mathbf{6}^+$ by [$\mathbf{2}^+$ + **3**] or [**2** + $\mathbf{3}^+$];
(c) doubly oxidized dumbbell $\mathbf{6}^{2+}$ by [$\mathbf{2}^{2+}$ + **3**] or [$\mathbf{2}^+$ + $\mathbf{3}^+$];
(d) neutral *green* isomer of [2]rotaxane **7** by [**4** + **3**];
(e) oxidized *green* isomer $\mathbf{7}^+$ by [$\mathbf{4}^+$ + **3**] or [**4** + $\mathbf{3}^+$];
(f) doubly oxidized *green* isomer $\mathbf{7}^{2+}$ by [$\mathbf{4}^{2+}$ + **3**] or [$\mathbf{4}^+$ + $\mathbf{3}^+$];
(g) neutral *red* isomer of [2]rotaxane **8** by [**2** + **5**];
(h) oxidized *red* isomer $\mathbf{8}^+$ by [$\mathbf{2}^+$ + **5**] or [**2** + $\mathbf{5}^+$];
(i) doubly oxidized *red* isomer $\mathbf{8}^{2+}$ by [$\mathbf{2}^{2+}$ + **5**] or [$\mathbf{2}^+$ + $\mathbf{5}^+$].

Since DNP has a higher reduction potential than TTF (section 3.3), we did not consider such unlikely combinations as [**2** + $\mathbf{3}^{2+}$], [**4** + $\mathbf{3}^{2+}$], and [**2** + $\mathbf{5}^{2+}$] for double oxidation.

In this bottom-up model, we ignore the linkers in **1**. Since the highest occupied molecular orbitals (HOMOs) of **1** are localized exclusively on the TTF or on DNP, the linkers connecting the two stations would not play an important role in oxidation, justifying this approach of ignoring them.

In this model, we also assume that the two stations do not *feel* each other. The assumption of no interaction between the two stations without any contact, coupling, or charge transfer (ultimately local oxidation) might appear too drastic, but this is justified as follows. First, the two stations in **1** are well separated from each other by an ethylene oxide linker as shown in section 4.1. Second, the two stations must be efficiently shielded from each other by a polar solvent (AN), as long as there is no direct $\pi-\pi$ type contact between them as confirmed in section 4.2.

2.2. Calculation Details. The initial structure of each component [TTF, DNP, CBPQT, $(TTF)(CBPQT)(PF_6)_4$, $(DNP)(CBPQT)(PF_6)_4$] is taken from X-ray crystallographic structures.[32−35]

First, we calculate the gas-phase ionization potentials of the simple dumbbell components, TTF and DNP, as well as their reduction potentials in AN, at various levels of theory (Table S1 in the Supporting Information) and compare with experimental data. We choose the following calculation scheme (Table S1d') which provides a good compromise between quality and cost for compounds as big as **4**−**5** and **7**−**8**.

A full geometry optimization in QM is carried out for each species in the gas phase using the B3LYP[36−40] flavor of DFT (unrestricted B3LYP for open-shell systems) with the 6-31G** basis set. At the final geometry, the gas-phase energy is upgraded using a larger basis set (B3LYP/6-311++G**), since the triple-ζ-quality basis set with diffusion functions has been shown to improve gas-phase electron detachment energies.[41,42] Despite the well-known issue that B3LYP may be inadequate to account for the dispersion interaction which is a significant contribution to the interaction between CBPQT and TTF/DNP,[16,19] it should still be adequate in describing the *difference* between the interactions at different oxidation states, since the variation of the dispersion interaction for different oxidation states should be minor compared to the variation of the electrostatic interaction. At the final geometry, the solvation energy in AN (dielectric constant 35.69, density 0.7857 g/cm^3 at 20 °C,[43] probe radius 2.18 Å) is also calculated in B3LYP/6-31G** (since the solvation energy is not very sensitive to the choice of basis set[42]) using the Poisson−Boltzmann continuum-solvation model.[44,45] The following atomic radii are used (in Å):[42] H 1.15, C 1.9, N 1.6, O 1.6, F 1.682, P 2.074, and S 1.7 (which has been changed from 1.9 to reproduce the experimental reduction potentials of TTF). All calculations are done using *Jaguar* v5.5.[46]

TABLE 1: Bottom-Up Model Components (in kcal/mol)

free[a]	ΔG°_{AN}	complexed[a,b]	ΔG°_{AN}
$\mathbf{2}^0$: $^1TTF^0$	−1144520.5	$\mathbf{4}^0$: $^1C(TTF^0)P$	−4516592.7
$\mathbf{2}^+$: $^2TTF^{\bullet+}$	−1144418.0	$\mathbf{4}^+$: $^2C(TTF^{\bullet+})P$	−4516478.5
$\mathbf{2}^{2+}$: $^1TTF^{2+}$	−1144302.2	$\mathbf{4}^{2+}$: $^1C(TTF^{2+})P$	−4516327.3
$\mathbf{3}^0$: $^1DNP^0$	−435347.3	$\mathbf{5}^0$: $^1C(DNP^0)P$	−3807408.2
$\mathbf{3}^+$: $^2DNP^{\bullet+}$	−435225.2	$\mathbf{5}^+$: $^2C(DNP^{\bullet+})P$	−3807278.7

[a] Superscripts on the left denote preferred spin states (singlet or doublet). The triplet states of the doubly oxidized components are less stable than the singlet states [$^3TTF^{2+}$ (−1144263.7) and $^3C(TTF^{2+})P$ (−4516302.7)]. [b] C(TTF)P = (CBPQT)(TTF)$(PF_6)_4$; C(DNP)P = (CBPQT)(DNP)$(PF_6)_4$.

For larger components, **4**−**5** and **7**−**8**, we skip geometry reoptimizations in solution phase since these optimizations for the smaller systems had little effect. We also skip the calculation of vibration frequencies, since such corrections for the simple TTF and DNP had little effect on the final results (<0.07 V in reduction potentials; Table S1), as suggested in an earlier study.[42] That is, although the free energy in solution of each species should be given as

$$\Delta G^\circ_{AN} = ZPE^{6-31G^*} + \Delta\Delta G_{0\rightarrow 298K}{}^{6-31G^{**}} + E_{0K,g}{}^{6-311++G^*} + \Delta G^\circ_{solv}{}^{6-31G^*},$$

we ignore the first two terms and use the simpler sum of the gas-phase energy (ΔE_g) and the solvation energy (ΔG_{solv}),

$$\Delta G^\circ_{AN} \cong \Delta E_g{}^{6-311++G^{**}} + \Delta G_{solv}{}^{6-31G^{**}} \quad (1)$$

2.3. Reduction Potential. The standard reduction potential (or oxidation potential) for a half-cell reaction

$$A^{n+} + e^- \rightarrow A^{(n-1)+}$$

with the free energy change

$$\Delta\Delta G^\circ_{red} = \Delta G^\circ[A^{(n-1)+}] - \Delta G^\circ[A^{n+}] \quad (2)$$

is given by

$$E^\circ_{1/2} = -\frac{\Delta\Delta G^\circ_{red}}{F} \quad (3)$$

where F is the Faraday constant (= eN_A = 1 eV/V). The experimental reduction potentials cited in the following sections are the values measured in AN with respect to the standard calomel electrode (SCE), whose electrode potential is 4.12 V. Thus, the calculated standard reduction potentials are also given with respect to SCE (in V): [42,47]

$$E^\circ = E^\circ_{1/2} - 4.12 \quad (4)$$

Since we do not find a drastic structural change after oxidation, we choose *vertical* oxidation for **4**−**5** and **7**−**8**; that is, we do not allow geometry relaxation after one or two electrons are removed from the corresponding neutral species.

3. Results

The gas-phase energies (ΔG°_g), the solvation energies in AN (ΔG°_{solv}), and the solution-phase energies (ΔG°_{AN}) of all relevant species are listed in Table S2 in the Supporting Information, as well as the charges/spins carried by TTF and DNP in those species.

Table 1 lists the solution-phase energies of bottom-up model components **2**−**5** at various oxidation states. Combining these component energies leads to the energies of the two-station models (**2** + **3**, **4** + **3**, and **2** + **5**) at various oxidation states (Tables 2−4). Comparing these combinations gives the preferred oxidation site (Tables 2−3) and the preferred ring position (Table 4) at each oxidation state.

TABLE 2: Oxidized Bottom-Up Models (in kcal/mol)

after 1st oxidation	spin	ΔG°_{AN}	$\Delta\Delta G^\circ_{AN}$
[2]Rotaxane (*Green* Isomer)			
$\mathbf{4}^+ + \mathbf{3}^0$: $C(TTF^{\bullet+})P + DNP^0$	doublet	**−4951825.7**	0.0
$\mathbf{4}^0 + \mathbf{3}^+$: $C(TTF^0)P + DNP^{\bullet+}$	doublet	−4951817.9	7.8
Dumbbell			
$\mathbf{2}^+ + \mathbf{3}^0$: $TTF^{\bullet+} + DNP^0$	doublet	−1579765.2	0.0
$\mathbf{2}^0 + \mathbf{3}^+$: $TTF^0 + DNP^{\bullet+}$	doublet	−1579745.6	19.6
[2]Rotaxane (*Red* Isomer)			
$\mathbf{2}^+ + \mathbf{5}^0$: $TTF^{\bullet+} + C(DNP^0)P$	doublet	**−4951826.2**	0.0
$\mathbf{2}^0 + \mathbf{5}^+$: $TTF^0 + C(DNP^{\bullet+})P$	doublet	−4951799.2	27.0

TABLE 3: Doubly Oxidized Bottom-Up Models (kcal/mol)

after 2nd oxidation	spin	ΔG°_{AN}	$\Delta\Delta G^\circ_{AN}$
[2]Rotaxane (*Green* Isomer)			
$\mathbf{4}^{2+} + \mathbf{3}^0$: $C(TTF^{2+})P + DNP^0$	singlet	−4951674.5	29.2
$\mathbf{4}^+ + \mathbf{3}^+$: $C(TTF^{\bullet+})P + DNP^{\bullet+}$	triplet[a]	**−4951703.7**	0.0
Dumbbell			
$\mathbf{2}^{2+} + \mathbf{3}^0$: $TTF^{2+} + DNP^0$	singlet	−1579649.4	0.0
$\mathbf{2}^+ + \mathbf{3}^+$: $TTF^{\bullet+} + DNP^{\bullet+}$	triplet[a]	−1579643.2	6.2
[2]Rotaxane (*Red* Isomer)			
$\mathbf{2}^{2+} + \mathbf{5}^0$: $TTF^{2+} + C(DNP^0)P$	singlet	**−4951710.4**	0.0
$\mathbf{2}^+ + \mathbf{5}^+$: $TTF^{\bullet+} + C(DNP^{\bullet+})P$	triplet[a]	−4951696.7	13.7

[a] Or singlet−triplet degenerate.

TABLE 4: Two Isomers of [2]Rotaxane (in kcal/mol)

	isomer	ΔG°_{AN}	$\Delta\Delta G^\circ_{AN}$
Neutral			
$\mathbf{4}^0 + \mathbf{3}^0$: $C(TTF^0)P + DNP^0$	*Green*	−4951939.9	0.0
$\mathbf{2}^0 + \mathbf{5}^0$: $TTF^0 + C(DNP^0)P$	*Red*	−4951928.7	11.2
Oxidized			
$\mathbf{4}^+ + \mathbf{3}^0$: $C(TTF^{\bullet+})P + DNP^0$	*Green*	−4951825.7	0.5
$\mathbf{2}^+ + \mathbf{5}^0$: $TTF^{\bullet+} + C(DNP^0)P$	*Red*	−4951826.2	0.0
Doubly Oxidized			
$\mathbf{4}^+ + \mathbf{3}^+$: $C(TTF^{\bullet+})P + DNP^{\bullet+}$	*Green*	−4951703.7	6.7
$\mathbf{2}^{2+} + \mathbf{5}^0$: $TTF^{2+} + C(DNP^0)P$	*Red*	−4951710.4	0.0

3.1. First Oxidation. Table 2 shows the relative energies of two different ways of the first oxidation: the oxidation at the TTF station ($\mathbf{2}^+ + \mathbf{3}^0$, $\mathbf{4}^+ + \mathbf{3}^0$, $\mathbf{2}^+ + \mathbf{5}^0$) and the oxidation at the DNP station ($\mathbf{2}^0 + \mathbf{3}^+$, $\mathbf{4}^0 + \mathbf{3}^+$, $\mathbf{2}^0 + \mathbf{5}^+$). As expected from the lower E° of TTF, the first oxidation occurs exclusively at the TTF station in all the cases. However, the preference of TTF over DNP as the oxidation site decreases in order of (TTF) + (CBPQT)(DNP)(PF_6) (**2** + **5**) > (TTF) + (DNP) (**2** + **3**) > (CBPQT)(TTF)$(PF_6)_4$ + (DNP) (**4** + **3**).

This is the same order as the energy gap between HOMO (TTF-character) and HOMO−1 (DNP-character) levels. Since the CBPQT ring exerts a net positive field on the station it encircles (DNP in **5**, TTF in **4**) stabilizing its orbital energy levels,[18] the HOMO level is higher (more available for oxidation) than HOMO-1 to the greatest extent in **2** + **5**, then in **2** + **3**, and in **4** + **3**.

This argument can also be interpreted simply in terms of the electrostatic repulsion between two positively charged moieties, the oxidation site (TTF^+ or DNP^+) and the ring ($CBPQT^{4+}$). This extra penalty of repulsion makes it more difficult to oxidize TTF when encircled with the ring (**4** + **3**) than when it is free (**2** + **3**). Likewise, it is more difficult to oxidize DNP when encircled with the ring (**2** + **5**) than when it is free (**2** + **3**).

Due to this repulsion, the preferred ring position may change after the first oxidation (Table 4). While the ring clearly prefers sitting on the TTF station ($\mathbf{4}^0 + \mathbf{3}^0$; *green* isomer) rather than on the DNP station ($\mathbf{2}^0 + \mathbf{5}^0$; *red* isomer) by 11.2 kcal/mol in the neutral state, the repulsion developed between TTF^+ and $CBPQT^{4+}$ after the first oxidation on TTF ($\mathbf{4}^+ + \mathbf{3}^0$) tends, if not completely, to drive the ring toward the DNP station ($\mathbf{2}^+ + \mathbf{5}^0$) with a very small energy preference of 0.5 kcal/mol.

The first oxidation is summarized as follows:

$$\mathbf{2}^0 + \mathbf{3}^0 \rightarrow \mathbf{2}^+ + \mathbf{3}^0 \quad \text{for dumbbell}$$

$$\mathbf{4}^0 + \mathbf{3}^0 \rightarrow [\mathbf{4}^+ + \mathbf{3}^0 \leftrightarrow \mathbf{2}^+ + \mathbf{5}^0] \text{ for [2]rotaxane}$$

3.2. Second Oxidation. Now, we consider the second oxidation. The oxidized dumbbell (TTF^+) + (DNP^0) ($\mathbf{2}^+ + \mathbf{3}^0$) prefers the second oxidation to be on TTF ($\mathbf{2}^{2+} + \mathbf{3}^0$) again rather than on DNP ($\mathbf{2}^+ + \mathbf{3}^+$) (Table 3). However, the TTF preference (6.2 kcal/mol) is smaller than in the first oxidation (19.6 kcal/mol). This is understood in terms of the orbital level shift. Like the stabilization effect due to the net positive field from the ring, the first oxidation (localized on TTF) creates a positive charge on TTF, leading to another significant stabilization on the TTF-character HOMO, while the level of the DNP-character HOMO−1 is unaltered.

For [2]rotaxane, one of the two first-oxidation products is the *red* isomer (TTF^+) + ($CBPQT)(DNP^0)(PF_6)_4$ ($\mathbf{2}^+ + \mathbf{5}^0$). The positive ring surrounding DNP makes DNP less available as the second oxidation site with its stabilization effect on the DNP-character HOMO−1. Moreover, the second oxidation on DNP ($\mathbf{2}^+ + \mathbf{5}^+$) would create an extra repulsion between the ring and DNP^+. Thus, in this *red* isomer, the second oxidation occurs preferentially on TTF, leading to $\mathbf{2}^{2+} + \mathbf{5}^0$ rather than $\mathbf{2}^+ + \mathbf{5}^+$, and the TTF preference is higher (13.7 kcal/mol) than in the dumbbell (6.2 kcal/mol) (Table 3).

The other first-oxidation product of [2]rotaxane is the *green* isomer ($CBPQT)(TTF^+)(PF_6)_4$ + (DNP^0) ($\mathbf{4}^+ + \mathbf{3}^0$). This isomer has a combined stabilization effect on the TTF-character HOMO; one is from the ring (encircling TTF), and the other is from the oxidation (localized on TTF). Thus, the TTF-character HOMO is even less available for the second oxidation. Moreover, the second oxidation on TTF ($\mathbf{4}^{2+} + \mathbf{3}^0$) would create a large penalty due to the repulsion between TTF^{2+} and the ring. Thus, in this *green* isomer, DNP is preferred as the second oxidation site by 29.2 kcal/mol, leading to $\mathbf{4}^+ + \mathbf{3}^+$ [open-shell ($CBPQT)(TTF^{\bullet+})(PF_6)_4$ + ($DNP^{\bullet+}$)] rather than $\mathbf{4}^{2+} + \mathbf{3}^0$ (Table 3).

However, the *green* isomer $\mathbf{4}^+ + \mathbf{3}^+$ is less stable than the *red* isomer $\mathbf{2}^{2+} + \mathbf{5}^0$ by 6.7 kcal/mol (Table 4). Thus, as long as the ring is free to move between the two stations, the second oxidation would not generate the open-shell *green* isomer $\mathbf{4}^+ + \mathbf{3}^+$. Instead, it should eventually induce a TTF-to-DNP ring shuttling, leading to $\mathbf{2}^{2+} + \mathbf{5}^0$.

The second oxidation is summarized as follows:

$$\mathbf{2}^+ + \mathbf{3}^0 \rightarrow \mathbf{2}^{2+} + \mathbf{3}^0 \quad \text{for dumbbell}$$

$$[\mathbf{4}^+ + \mathbf{3}^0 \leftrightarrow \mathbf{2}^+ + \mathbf{5}^0] \rightarrow \mathbf{2}^{2+} + \mathbf{5}^0 \text{ for [2]rotaxane}$$

3.3. Reduction Potential. The calculated reduction potentials are listed in Table 5 along with the experimental values.

From the experiment, a free TTF, including a TTF attached to ethylene oxide linkers (control compound), is known to have an E°_1 of 0.3−0.4 V and an E°_2 of 0.7−0.8 V.[10,30,31,48,49] (An E°_1 as high as 0.5 and 0.66 V has also been reported for a free TTF station in the metastable state of rotaxane and catenane.[13]) When the TTF is encircled by the ring in a rotaxane or pseudorotaxane [$(CBPQT)(TTF)(PF_6)_4$], the E°_1 moves up especially at a high CV scan rate so that the two single-electron oxidations (E°_1 and E°_2) merge into a single bi-electronic oxidation occurring at 0.7−0.9 V.[10,13,30,31] (This can also be as high as 1.00 V for catenane.[13]) A free DNP is known to have E°_1 of 1.1−1.3 V,[10,31,50,51] but when it is encircled by the ring in the metastable state of rotaxane, it moves up to 1.65 V (certainly higher than 1.30 V).[10,31] For the dumbbell compound with ethylene oxide linkage between TTF and DNP, the oxidation occurs at 0.28−35, 0.70−0.73, and 1.17−1.18 V without evidence of intercomponent interaction.[10,31]

TABLE 5: Reduction Potentials (E° vs SCE; in V) in Acetonitrile

bottom-up model	E°_1	E°_2	E°_3	E° (expt)[a]
2: TTF	0.32	0.90		0.3−0.4; 0.7−0.8
3: DNP	1.18			1.1−1.3
4: C(TTF)P	0.83	2.44		0.7−1.0
5: C(DNP)P	1.49			1.65, >1.30
TTF + DNP	0.32	0.90	1.17	0.2−0.4; 0.7−0.8; 1.1−1.2
C(TTF)P + DNP	0.81	0.90		0.7−1.0; 0.7−1.0

[a] See text (section 3.3).

TABLE 6: Dumbbell with Different Lengths of Linkers

dumbbell models	Δ(S − T)[a]	E°_1 (V)	E°_2 (V)
(a) TTF−DNP (**6a**)	1.1 (S)	0.40	1.15
(b) TTF−OCH_2CH_2O−DNP (**6b**)	4.2 (S)	0.34	1.04
(c) TTF−$O(CH_2CH_2O)_2$−DNP	4.3 (S)	0.36	1.03
(d) TTF + DNP (**2** + **3**)	6.2 (S)	0.32	0.90

[a] Singlet−triplet energy difference in the doubly oxidized state (kcal/mol) and the preferred spin state.

For the bottom-up components **2**−**5**, the calculated E°s are in a reasonable agreement with experiments: 0.32 and 0.90 V for **2**, 1.18 V for **3**, 0.83 V for **4**, and 1.49 V for **5**.

For the composite two-station models (**2** + **3**, **4** + **3**, **2** + **5**), in this bottom-up approach, the calculated E°s are just those of the separate components involved in the corresponding oxidation processes.

For the dumbbell **2** + **3**, the oxidation occurs on TTF first ($\mathbf{2}^+ + \mathbf{3}^0$), then on TTF again ($\mathbf{2}^{2+} + \mathbf{3}^0$), and then on DNP ($\mathbf{2}^{2+} + \mathbf{3}^+$). Thus, its E°s are calculated as 0.32 (E°_1 of TTF), 0.90 (E°_2 of TTF), and 1.17 V (E°_1 of DNP), in agreement with experiment values.[10,31]

For [2]rotaxane, the first oxidation occurs at the ring-encircled TTF of the *green* isomer **4** + **3**, leading to $\mathbf{4}^+ + \mathbf{3}^0$ in close equilibrium with the *red* isomer $\mathbf{2}^+ + \mathbf{5}^0$. Thus, its E°_1 is calculated as 0.81 V (close to the E°_1 of **4**). Then, the second oxidation occurs at the free TTF of the *red* isomer $\mathbf{2}^+ + \mathbf{5}^0$, leading exclusively to $\mathbf{2}^{2+} + \mathbf{5}^0$. Thus, the E°_2 is calculated as 0.90 V (close to the E°_2 of **2**). These two reduction potentials are closer to each other (0.81 and 0.90 V) than those of the dumbbell (0.32 and 0.90 V), in agreement with the experimental results.[13,30,31]

4. Discussion: Validity of Bottom-up Model

The validity of our bottom-up model relies on the assumption of no interaction between the two stations without any coupling or contact.

4.1. Linker. To see how much coupling exists between the two stations through the ethylene oxide linker (−OCH_2CH_2O−), we compared three different models of dumbbells having different lengths of linkers (Table 6):

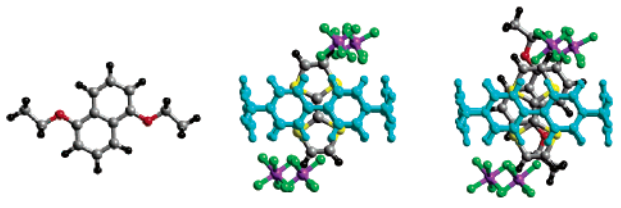

Figure 3. $\pi-\pi$ association between (CBPQT)(TTF)$(PF_6)_4$ and DNP, which was calculated to be endothermic in the acetonitrile solution but exothermic in the gas phase.

(a) the shortest, direct connection, TTF−DNP (**6a**);
(b) the actual connection in **1**, TTF−OCH_2CH_2O−DNP **(6b)**;
(c) a longer connection, TTF−$O(CH_2CH_2O)_2$−DNP;
(d) the asymptotic connection (bottom-up model; **2** + **3)**.

The singlet−triplet energy difference of the doubly oxidized dumbbell is closely related to the degree of coupling between the two stations. The bottom-up model (d) gives a similar result as the model with the actual connection in **1** (b).

4.2. $\pi-\pi$ Contact. Even when the linker is long enough to avoid a coupling between the two stations, its flexibility might allow a $\pi-\pi$-type contact between the two stations in a folded conformation. However, we calculate that the $\pi-\pi$ association of two stations, (CBPQT)(TTF)$(PF_6)_4$ and DNP [**3** + **4** → **9**, Figure 3], is endothermic in AN [$\Delta\Delta G^\circ_{AN}$ = 9.6 kcal/mol, Table S1] showing a fairly large desolvation penalty [$\Delta\Delta G^\circ_{solv}$ = 12.4 kcal/mol] upon losing a contact between a polar paraquat face of the $CBPQT^{4+}$ ring and the solvent. This indicates that the stations should be apart from each other in AN, justifying our bottom-up approach in studying solution-phase behaviors such as reduction potentials.

However, the exothermic nature of this $\pi-\pi$ association in the gas phase [$\Delta\Delta G^\circ_g = -2.9$ kcal/mol] implies that a direct contact between the two stations might be more important in such nonpolar environments as in solid-state devices, perhaps requiring a full two-station model for accurate descriptions of the switching behaviors. To consider this case in which the two stations communicate with each other, we employed a directly connected two-station model, **6**−**8**, to allow a coupling or a charge flow between the two stations (Table S2 in the Supporting Information). The consequence of this direct coupling is that the positive charges created after oxidation are distributed over both stations, favoring the open-shell triplet state for the doubly oxidized species: $(TTF^{\bullet+})-(DNP^{\bullet+})$ (^{3}**6b**$^{2+}$), (CBPQT)-$(TTF^{\bullet+})(PF_6)_4-(DNP^{\bullet+})$ (^{3}**7**$^{2+}$), $(TTF^{\bullet+})-$(CBPQT)$(DNP^{\bullet+})$-$(PF_6)_4$ (^{3}**8**$^{2+}$). Then, we do not expect any driving force for the TTF-to-DNP ring shuttling. Indeed, this model prefers the *green* isomer **7** to the *red* isomer **8** irrespective of the oxidation state, without any indication of the ring shuttling. This implies that, in a nonpolar medium where [2]rotaxane might form a $\pi-\pi$ contact between the two stations, the switching upon the double oxidation of [2]rotaxane might not involve a TTF-to-DNP ring shuttling but rather a transition from a closed-shell system (^{1}**7**^{0}) to a $\pi-\pi$ stacked open-shell system (^{3}**7**$^{2+}$).

4. Summary

The oxidation of the central components of the Stoddart−Heath [2]rotaxane molecular switch in AN was studied using DFT (B3LYP) and the Poisson−Boltzmann continuum-solvation model. The calculations in a bottom-up approach support the hypothesis proposed from experiments. The first oxidation occurs on TTF leading to the $[TTF^+-DNP^0]$ type configuration (Table 2). The repulsion between TTF^+ and $CBPQT^{4+}$ tends to drive the $CBPQT^{4+}$ ring from the TTF^+ station toward the neutral DNP station, but this is not dominant (Table 4). After the second oxidation, however, [2]rotaxane clearly prefers a $[TTF^{2+}-DNP^0]$ type configuration where the $CBPQT^{4+}$ ring has been moved from the TTF^{2+} station to the DNP station (Tables 3 and 4). This process makes the two reduction potentials of [2]rotaxane very close, 0.81 and 0.90 V, compared to those of the dumbbell, 0.32 and 0.90 V (as observed experimentally). This good agreement from the bottom-up model indicates that the two stations are well separated or shielded from each other in AN solution. However, in such nonpolar environments as solid-state devices, a direct contact between the two stations might be more important, perhaps requiring a full two-station model for accurate descriptions of the switching behaviors.

Acknowledgment. We thank Dr. Seung Soon Jang, Dr. Yong-Hoon Kim, the Prof. J. Fraser Stoddart group at UCLA, and the Prof. James Heath group of Caltech for helpful discussions. This work was initiated with support by the National Science Foundation [NIRT] and continued with support from MARCO-FENA. In addition, the facilities of the MSC were supported by ONR-DURIP, ARO-DURIP, and NSF-MRI.

Supporting Information Available: Basis set dependence of calculation results on TTF/DNP (Table S1) and a master table listing the solution-phase energies of all relevant species and the charges/spins carried by TTF and DNP in those species at each oxidation step (Table S2). This material is available free of charge via the Internet at http://pubs.acs.org.

References and Notes

(1) Carroll, R. L.; Gorman, C. B. *Angew. Chem., Int. Ed.* **2002**, *41*, 4378−4400.
(2) Heath, J. R.; Ratner, M. A. *Phys. Today* **2003**, *56*, 43−49.
(3) Reed, M. A.; Tour, J. M. *Sci. Am.* **2000**, *282*, 86−93.
(4) Luo, Y.; Collier, C. P.; Jeppesen, J. O.; Nielsen, K. A.; Delonno, E.; Ho, G.; Perkins, J.; Tseng, H.-R.; Yamamoto, T.; Stoddart, J. F.; Heath, J. R. *ChemPhysChem* **2002**, *3*, 519−525.
(5) Collier, C. P.; Wong, E. W.; Belohradsky, M.; Raymo, F. M.; Stoddart, J. F.; Kuekes, P. J.; Williams, R. S.; Heath, J. R. *Science* **1999**, *285*, 391−394.
(6) Wong, E. W.; Collier, C. P.; Behloradsky, M.; Raymo, F. M.; Stoddart, J. F.; Heath, J. R. *J. Am. Chem. Soc.* **2000**, *122*, 5831−5840.
(7) Flood, A. H.; Stoddart, J. F.; Steuerman, D. W.; Heath, J. R. *Science* **2004**, *306*, 2055−2056.
(8) Collier, C. P.; Mattersteig, G.; Wong, E. W.; Luo, Y.; Beverly, K.; Sampaio, J.; Raymo, F. M.; Stoddart, J. F.; Heath, J. R. *Science* **2000**, *289*, 1172−1175.
(9) Pease, A. R.; Jeppesen, J. O.; Stoddart, J. F.; Luo, Y.; Collier, C. P.; Heath, J. R. *Acc. Chem. Res.* **2001**, *34*, 433−444.
(10) Balzani, V.; Credi, A.; Mattersteig, G.; Matthews, O. A.; Raymo, F. M.; Stoddart, J. F.; Venturi, M.; White, A. J. P.; Williams, D. J. *J. Org. Chem.* **2000**, *65*, 1924−1936.
(11) Tseng, H.-R.; Vignon, S. A.; Stoddart, J. F. *Angew. Chem., Int. Ed.* **2003**, *42*, 1491−1495.
(12) Nikitin, K.; Fitzmaurice, D. *J. Am. Chem. Soc.* **2005**, *127*, 8067−8076.
(13) Flood, A. H.; Peters, A. J.; Vignon, S. A.; Steuerman, D. W.; Tseng, H.-R.; Kang, S.; Heath, J. R.; Stoddart, J. F. *Chem.—Eur. J.* **2004**, *10*, 6558−6564.
(14) Steuerman, D. W.; Tseng, H.-R.; Peters, A. J.; Flood, A. H.; Jeppesen, J. O.; Nielsen, K. A.; Stoddart, J. F.; Heath, J. R. *Angew. Chem., Int. Ed.* **2004**, *43*, 6486−6491.
(15) Kim, Y.-H.; Jang, S. S.; Jang, Y. H.; Goddard, W. A., III *Phys. Rev. Lett.* **2005**, *94*, 156801.
(16) Romero, C.; Fomina, L.; Fomine, S. *Int. J. Quantum Chem.* **2005**, *102*, 200−208.
(17) Deng, W.-Q.; Muller, R. P.; Goddard, W. A., III *J. Am. Chem. Soc.* **2004**, *126*, 13562−13563.
(18) Jang, Y. H.; Hwang, S.; Kim, Y.-H.; Jang, S. S.; Goddard, W. A., III *J. Am. Chem. Soc.* **2004**, *126*, 12636−12645.
(19) Ercolani, G.; Mencarelli, P. *J. Org. Chem.* **2003**, *68*, 6470−6473.

(20) Zhang, K.-C.; Liu, L.; Mu, T.-W.; Guo, Q.-X. *Chem. Phys. Lett.* **2001**, *333*, 195−198.
(21) Macias, A. T.; Kumar, K. A.; Marchand, A. P.; Evanseck, J. D. *J. Org. Chem.* **2000**, *65*, 2083−2089.
(22) Castro, R.; Berardi, M. J.; Cordova, E.; de Olza, M. O.; Kaifer, A. E.; Evanseck, J. D. *J. Am. Chem. Soc.* **1996**, *118*, 10257−10268.
(23) Ceccarelli, M.; Mercuri, F.; Passerone, D.; Parrinello, M. *J. Phys. Chem. B* **2005**, *109*, 17094−17099.
(24) Jang, Y. H.; Jang, S. S.; Goddard, W. A., III *J. Am. Chem. Soc.* **2005**, *127*, 4959−4964.
(25) Jang, S. S.; Jang, Y. H.; Kim, Y.-H.; Goddard, W. A., III; Flood, A. H.; Laursen, B. W.; Tseng, H.-R.; Stoddart, J. F.; Jeppesen, J. O.; Choi, J. W.; Steuerman, D. W.; DeIonno, E.; Heath, J. R. *J. Am. Chem. Soc.* **2005**, *127*, 1563−1575.
(26) Grabuleda, X.; Ivanov, P.; Jaime, C. *J. Org. Chem.* **2003**, *68*, 1539−1547.
(27) Zheng, X.; Sohlberg, K. *J. Phys. Chem. A* **2003**, *107*, 1207−1215.
(28) Kaminski, G. A.; Jorgensen, W. L. *J. Chem. Soc., Perkin Trans. 2* **1999**, 2365−2375.
(29) Grabuleda, X.; Jaime, C. *J. Org. Chem.* **1998**, *63*, 9635−9643.
(30) Liu, Y.; Flood, A. H.; Stoddart, J. F. *J. Am. Chem. Soc.* **2004**, *126*, 9150−9151.
(31) Tseng, H.-R.; Vignon, S. A.; Celestre, P. C.; Perkins, J.; Jeppesen, J. O.; Fabio, A. D.; Ballardini, R.; Gandolfi, M. T.; Venturi, M.; Balzani, V.; Stoddart, J. F. *Chem.—Eur. J.* **2004**, *10*, 155−172.
(32) Philp, D.; Slawin, A. M. Z.; Spencer, N.; Stoddart, J. F.; Williams, D. J. *J. Chem. Soc., Chem. Commun.* **1991**, 1584−1586.
(33) Reddington, M. V.; Slawin, A. M. Z.; Spencer, N.; Stoddart, J. F.; Vincent, C.; Williams, D. J. *J. Chem. Soc., Chem. Commun.* **1991**, 630−634.
(34) Odell, B.; Reddington, M. V.; Slawin, A. M. Z.; Spencer, N.; Stoddart, J. F.; Williams, D. J. *Angew. Chem., Int. Ed. Engl.* **1988**, *27*, 1547−1550.
(35) Anelli, P. L.; Ashton, P. R.; Ballardini, R.; Balzani, V.; Delgado, M.; Gandolfi, M. T.; Goodnow, T. T.; Kaifer, A. E.; Philp, D.; Pietraszkiewicz, M.; Prodi, L.; Reddington, M. V.; Slawin, A. M. Z.; Spencer, N.; Stoddart, J. F.; Vicent, C.; Williams, D. J. *J. Am. Chem. Soc.* **1992**, *114*, 193−218.
(36) Slater, J. C. *Quantum Theory of Molecules and Solids. Vol. 4. The Self-Consistent Field for Molecules and Solids*; McGraw-Hill: New York, 1974.
(37) Becke, A. D. *Phys. Rev. A* **1988**, *38*, 3098−3100.
(38) Vosko, S. H.; Wilk, L.; Nusair, M. *Can. J. Phys.* **1980**, *58*, 1200−1211.
(39) Lee, C.; Yang, W.; Parr, R. G. *Phys. Rev. B* **1988**, *37*, 785−789.
(40) Miehlich, B.; Savin, A.; Stoll, H.; Preuss, H. *Chem. Phys. Lett.* **1989**, *157*, 200−206.
(41) Jang, Y. H.; Goddard, W. A., III; Noyes, K. T.; Sowers, L. C.; Hwang, S.; Chung, D. S. *J. Phys. Chem. B* **2003**, *107*, 344−357.
(42) Baik, M.-H.; Friesner, R. A. *J. Phys. Chem. A* **2002**, *106*, 7407−7412.
(43) Lide, D. R. *CRC Handbook of Chemistry and Physics*, 84th ed.; CRC Press: Boca Raton, FL, 2003−2004.
(44) Tannor, D. J.; Marten, B.; Murphy, R.; Friesner, R. A.; Sitkoff, D.; Nicholls, A.; Ringnalda, M. N.; Goddard, W. A., III; Honig, B. A. *J. Am. Chem. Soc.* **1994**, *116*, 11875−11882.
(45) Marten, B.; Kim, K.; Cortis, C.; Friesner, R. A.; Murphy, R. B.; Ringnalda, M. N.; Sitkoff, D.; Honig, B. *J. Phys. Chem.* **1996**, *100*, 11775−11788.
(46) *Jaguar 5.5*; Schrodinger Inc.: Portland, OR, 2003.
(47) Winget, P.; Cramer, C. J.; Truhlar, D. G. *Theor. Chem. Acc.* **2004**, *112*, 217−227.
(48) Coffen, D. L.; Chambers, J. Q.; Williams, D. R.; Garret, P. E.; Canfield, N. D. *J. Am. Chem. Soc.* **1971**, *93*, 2258−2268.
(49) Asakawa, M.; Ashton, P. R.; Balzani, V.; Credi, A.; Mattersteig, G.; Mattews, O. A.; Montalti, M.; Spencer, N.; Stoddart, J. F.; Venturi, M. *Chem.—Eur. J.* **1997**, *3*, 1992−1996.
(50) Zweig, A.; Maurer, A. H.; Roberts, B. G. *J. Org. Chem.* **1967**, *32*, 1322−1329.
(51) Ashton, P. R.; Baldoni, V.; Balzani, V.; Claessens, C. G.; Credi, A.; Hoffmann, H. D. A.; Raymo, F. M.; Stoddart, J. F.; Venturi, M.; White, A. J. P.; Williams, D. J. *Eur. J. Org. Chem.* **2000**, 1121−1130.